Cell Biology International ISSN 1065-6995
doi: 10.1002/cbin.11268

RESEARCH ARTICLE

In silico and in vitro effects of the I30T mutation on myelin protein zero instability in the cell membrane

Fatemeh Ghanavatinejad[1], Zahra Pourteymourfard-Tabrizi[1], Karim Mahnam[2], Abbas Doosti[3], Ameneh Mehri-Ghahfarrokhi[4], Masoumeh Pourhadi[1], Sayedeh Azimeh Hosseini[1], Morteza Hashemzadeh Chaleshtori[1], Payam Soltanzadeh[5] and Mohammad-Saeid Jami[1,5]*

1 Cellular and Molecular Research Center, Basic Health Sciences Institute, Shahrekord University of Medical Science, Shahrekord, Iran
2 Department of Biology, Faculty of Science, Shahrekord University, Rahbar Blvd, Shahrekord, Chaharmahal and Bakhtiari Province, Iran
3 Biotechnology Research Center, School of Basic Sciences, Islamic Azad University, Shahrekord Branch, Rahmatieh, Shahrekord, Chaharmahal and Bakhtiari Province, Iran
4 Department of Molecular Medicine, School of Advanced Technologies, Shahrekord University of Medical Sciences, Rahmatieh, Shahrekord, Chaharmahal and Bakhtiari Province, Iran
5 Department of Neurology, David Geffen School of Medicine, University of California Los Angeles (UCLA), 710 Westwood Plaza, Los Angeles, California, 90095, USA

Abstract

Charcot-Marie-Tooth (CMT) diseases are a heterogeneous group of genetic peripheral neuropathies caused by mutations in a variety of genes, which are involved in the development and maintenance of peripheral nerves. Myelin protein zero (MPZ) is expressed by Schwann cells, and MPZ mutations can lead to primarily demyelinating polyneuropathies including CMT type 1B. Different mutations demonstrate various forms of disease pathomechanisms, which may be beneficial in understanding the disease cellular pathology. Our molecular dynamics simulation study on the possible impacts of I30T mutation on the MPZ protein structure suggested a higher hydrophobicity and thus lower stability in the membranous structures. A study was also conducted to predict native/mutant MPZ interactions. To validate the results of the simulation study, the native and mutant forms of the MPZ protein were separately expressed in a cellular model, and the protein trafficking was chased down in a time course pattern. In vitro studies provided more evidence on the instability of the MPZ protein due to the mutation. In this study, qualitative and quantitative approaches were adopted to confirm the instability of mutant MPZ in cellular membranes.

Keywords: CMT1B; MPZ; mutation; molecular dynamics simulation; trafficking

Introduction

Polyneuropathies are relatively common disorders of the peripheral nervous system. Genetic and acquired neuropathies each contribute to one-third of these sets of disorders (Burns and Mauermann, 2011). Due to the impact on a particular protein, the hereditary polyneuropathies represent a valuable source to understand the demyelinating mechanisms, which are usually associated with impaired nerve conduction velocity. However, acquired polyneuropathies are linked with random demyelination, asymmetric nerve conduction velocities accompanied by blocked transmission and temporal propagation (Verhamme, 2010). Charcot-Marie Tooth disease (CMT) is a group of heterogeneous, nonsyndromic, and genetically inherited disorders of the peripheral nervous system involving over 90 genes with a global prevalence of 1 per 2,500 in most populations (DiVincenzo et al., 2014). A slowly progressive usually painless loss of sensation and distal muscle weakness and atrophy are hallmarks of these set of disorders. CMTs are classified based on the pattern of inheritance, primary involvement of the axon or myelin sheath, and the culprit genes. Ulnar motor conduction velocity slower than 38 m/s is used as a criterion for primary demyelinating CMTs (Type 1) (Braathen et al., 2011; Rossor et al., 2013) and velocities faster than 45 m/s are considered normal and hence a likely axonal variant (CMT2) (Berger et al., 2006; Niemann et al., 2006).

*Corresponding author: e-mail: saeidjami@mednet.ucla.edu

Abbreviations: ASA, accessible surface area; CHO-K1, Chinese Hamster Ovary cells; CMT, Charcot-Marie Tooth; DMEM, Dulbecco's minimum essential medium; MBP, maltose binding protein; NCV, nerve conduction velocity; PDB, Protein Data Bank; RMSD, root mean square deviation; *MPZ*, myelin protein zero; MD, molecular dynamics simulation; PCA, principal component analysis; Rg, radius of gyration; RMSF, root mean square fluctuation

Over 200 different mutations have been reported in the *MPZ* gene in 1q22-23 (Bai et al., 2018). *MPZ* mutations present with a wide range of clinical phenotypes from a severe infantile form so-called the "Dejerine-Sottas syndrome" to a benign late-onset phenotype of CMT2 with no major slowing of the conduction velocity. Most *MPZ* mutations have been found in the extracellular domain of MPZ, where it provides homophilic interactions with adjacent cis and trans-MPZs to keep two opposite leaflets of myelin membrane close to each other (Shy et al., 2004). According to genotype–phenotype studies, disruption of compact myelin assembly in the prenatal stage with early manifestation of the disease phenotypes is characteristic of the first group of *MPZ* mutations that disrupt intracellular trafficking of the MPZ protein.

Conversely, the mutant MPZ can be transported to the plasma membrane and contributes to the myelin sheath structures and despair the normal compact myelin structure via dominant-negative effects of mutant/wild-type MPZ interactions. The other group is known by normal or moderately reduced NCV, followed by severe axonopathy and late-onset of disease (Berger et al., 2007). Cellular pathomechanism is still unclear regarding the expiration of *MPZ* expression in post-natal neurons (Berger et al., 2007).

Mutations in the MPZ protein cause dramatic changes in the myelin sheath surrounding peripheral axons. A disordered myelin sheath disturbs Schwann cell-axon interactions and nerve signal conduction (Ghasemi-Dehkordi et al., 2015; Mahmoudian-sani et al., 2017; Ghanavatinejad et al., 2019; Mehri-Ghahfarrokhi et al., 2019; Rafiee et al., 2019). In other words, it affects the whole peripheral nervous system in patients with these mutations, and yet there is no comprehensive explanation for the disease pathomechanism.

In silico methods help to understand the effect of mutations on the structure and function of proteins. Molecular dynamics simulations have evolved into a mature technic that can be used effectively to understand macromolecular structure/function relationships (Mosaeilhy et al., 2017; Thirumal Kumar et al., 2018). These approaches mimic and predict the structure of macromolecules according to their atomic properties. For a fixed period, the molecules and atoms are allowed to interact, proposing a dynamic evolution of the system. Therefore, these approaches are excellent tools to predict the structure of proteins, especially when analyzing the effects of a particular mutation (Hospital et al., 2015).

In this study, we analyzed a transition mutation in the 89th nucleotide of the second exon of the *MPZ* gene, which alters the Isoleucine amino acid to Threonine in the 30th position of the extracellular domain of MPZ (I30T). We have performed an In silico analysis to predict protein thermodynamic variations due to the mutation. As the mutation is located at the first amino acid after the signal peptide (29 amino acids) we investigated whether the mutation can affect MPZ trafficking and integration into the cell membrane. Therefore, to pursue cellular and molecular basis of nerve damage caused by this mutation, native and mutant protein were separately expressed in the Chinese Hamster Ovary cell (CHO-K1) cellular model, and MPZ trafficking was followed during a time course to investigate the impact of the mutation on the trafficking.

Experimental procedure

Patients reports

A total number of 58 families diagnosed with CMT in the provinces of Isfahan and Chaharmahal-Bakhtiari (Iran) were studied. Nerve Conduction Velocity (NVC) was carefully evaluated and recorded (according to the ethics guidelines of Shahrekord University of Medical Sciences) for all patients at the EMG-NCV center at Al-Zahra hospital (Isfahan, Iran). The study was approved by the committee of ethics at the Deputy of Research And Technology of Shahrekord University of Medical Sciences.

Molecular analysis

After informed consent, peripheral blood samples were obtained from patients, and the DNA samples were isolated from the whole blood by DNA extraction kit (CinnaGen, Iran). Mutation screening of the *MPZ* gene was conducted after polymerase chain reaction (PCR) amplification of the entire coding regions (Table 1). PCR was performed in a final volume of 50 μL in 0.2 mL tubes containing 50 ng of purified DNA, 500 nM of each forward and reverse primer, 2 mM MgCl2, 200 mM dNTPs, 5 μL of 10× reaction buffers and 1 unit of Taq DNA polymerase (all from Thermo Fisher Scientific, Freiburg, Germany). The amplifications were carried out in a Thermal Cycler (Mastercycler Gradient; Eppendorf, Germany). The temperature profiles started with an initial denaturation step at 94°C for 5 min, followed by 35 cycles of the denaturation step at 94°C for 1 min, a primer-annealing step at 60°C for 1 min, extension step at 72°C for 1 min, and then a final step at 72°C for 5 min. To confirm the specificity, the amplified products were evaluated on 1% agarose gel electrophoresis, and the PCR products were analyzed with an ABI sequencing instrument.

Molecular modeling

On the basis of the results obtained from experimental methods, we selected the I30T mutant for theoretical study. This position is highly conserved in MPZ protein and located in the immunoglobulin-like domain, which is responsible for extracellular interaction with other proteins or molecules. The

Table 1 List of all primers used to perform polymerase chain reaction (PCR) and sequencing analysis of myelin protein zero (MPZ) exons.

Primer	Genes	Sequence 5′-3′	Product (bp)
1	MPZ-Exon 1-F	GCTGCAATTGGTTACTGGC	290
	MPZ-Exon 1-R	AGTGCAGCAAAGGCTGTG	
2	MPZ-Exon 2-F	CCCAATCTCTGGAAGTCCTC	472
	MPZ-Exon 2-R	GCACTTTCTGTTATCCAACCC	
3	MPZ-Exon 3-F	GCTTTGACAGCTGTGTTCTCA	344
	MPZ-Exon 3-R	CCAACCTATCAGTCCTCCCT	
4/5	MPZ-Exon 4/5-F	GACTAGGAACCACAGATACAGGG	534
	MPZ-Exon 4/5-R	ACACATCAGTCACCGAGCG	
6	MPZ-Exon 6-F	GTGGGATGGGAACAGTCAA	1376
	MPZ-Exon 6-R	GAAGGTTGGGGATGGGATA	
8	Albumin-F	TGTTGCATGAGAAAACGCCA	72
	Albumin-R	GTCGCCTGTTCACCAAGGAT	

sequence of the MPZ protein consisting of 248 residues was extracted from the UniProt website (isoform 1: P25189-1). Human MPZ consists of three domains, including an extracellular domain (residues 1–153), a transmembrane domain (residues 154–179), and a cytoplasmic domain (residues 180–248). Considering MPZ being a hydrophobic membrane protein, the full structure of this protein has not been yet provided by the Protein Data Bank (PDB). Only the crystallographic structure of the extracellular domain of MPZ has been provided by PDB via Maltose Binding Protein (MBP) (386 residues, PDB code: 3OAI), but the three-dimensional (3D) structure of whole MPZ protein does not exist. This PDB structure is 100% identical to the extracellular domain of MPZ protein. Figure 1 shows the alignment of the extracellular part

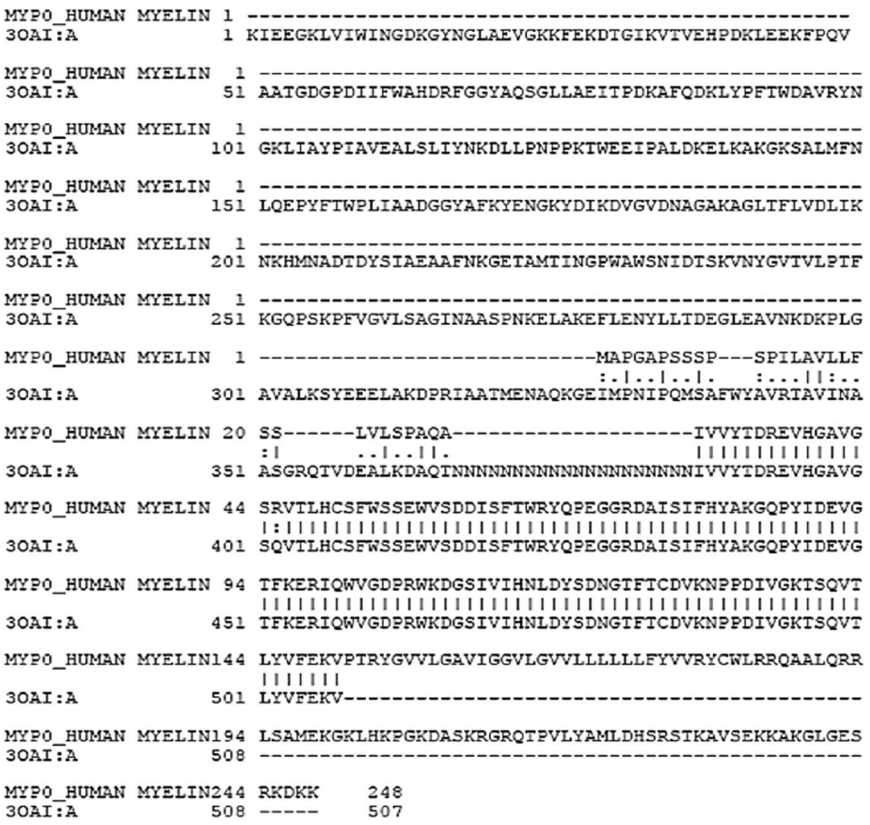

Figure 1 Alignment of the extracellular part of myelin protein zero (MPZ) (30–150) with the C-terminal part of the fusion protein 3OAI (378–447) to confirm the complete identity of the extracellular region.

of the MPZ protein (30–150) with the C-terminal part of 3OAI (387–507).

As a template for transmembrane and cytoplasmic domains of MPZ protein is not available, and the mutation has occurred in the extracellular part of MPZ, we only made the 3D structure of the extracellular part of MPZ. Five thousand models were built for native protein with Modeler 9 software (Šali and Blundell, 1993). The best model with the least normalized DOPE energy was selected. A Ramachandran plot was drawn with Rampage server, and the percentage of the residues in the allowed and disallowed regions was obtained. Eventually, residues 1–29 were removed from the model because these residues belonged to the signal peptide, which is removed during the entrance of MPZ to the membrane, and this sequence would not contribute to the final structure of the protein. The obtained structures were used for the MD simulation study. Also, residue Ile 1 was substituted with Thr via SPDV viewer software and used for MD simulation of the mutant sequence to investigate the impact of mutation at the molecular level and protein folding.

Molecular dynamics simulation

Molecular dynamics simulation was performed with the GROMACS 5 package (Berendsen et al., 1995; Lindahl et al., 2001; Van Der Spoel et al., 2005; Hess et al., 2008) under G43a1 force field and TIP4P water model. The full MPZ protein was embedded in a box containing 19,000 water molecules. The total charge of protein was +11e, and the number of Na^+ and Cl^- ions were 43 and 54, respectively, to reach the total charge of zero and the ionic strength of 140 mM (Saffar et al., 2015). The ionic strength of 140 mM is similar to the ionic strength of cells (van Oss, 2008), and the positive charge of MPZ protein helps its localization to the membrane. MD simulation was conducted for 100 ns in the NPT ensemble and 300 K with the Parrinello-Rahman barostat coupling algorithm (Mansourian et al., 2012). All protein bond lengths were constrained using the LINCS algorithm (Hess et al., 1997) and the time step of 1 fs for both native and mutant MPZ protein and with the same procedure as stated in our earlier work (Mansourian et al., 2012). The secondary structural elements of the protein were calculated by do_dssp, which utilizes the dssp utility during MD simulation. Principal component analysis (PCA) was performed using gmx covar and gmx anaeig and gmx sham modules of the GROMACS 5 package.

Docking

MPZ protein makes the dimer or tetramer form in the membrane of the Schwann cells. To evaluate the effect of the mutation on the interaction of MPZ monomers, the final monomer structure obtained from 100 ns MD simulation was used for docking simulation via the Haddock server (http://haddock.science.uu.nl/services/HADDOCK/haddockserver-easy.html) (Van Zundert et al., 2016). This server can dock two native or mutant monomers of the MPZ structure to each other and provides a better understanding of the effect of the mutation on the dimerization of the MPZ protein. Residue Ile 1 (or Thr 1 in the mutant form) and Asn 87 were considered as active residues for the Haddock server in both native and mutant MPZ proteins.

Cell culture

CHO-K1 cells were cultured and expanded in DMEM/F12 (Dulbecco's minimum essential medium, Gibco, UK) media supplemented with 10% inactivated fetal bovine serum (Gibco, UK) and 1% PnsStrep (Gibco) at 37°C under an atmosphere of 5% CO_2/95% air. Cells were seeded in tissue culture plates (SPL, Korea) for 48 h until the cell density reached 70% before being subjected to each experiment.

Vector design, cloning, and transfection

The complementary DNA (cDNA) sequence of the native *MPZ* gene from Ensemble databank (https://asia.ensembl.org) was cloned between the *Bam*HI and *Eco*RI restriction sites of the pCDNA3.1(+) expression vector. For the expression of the Mutant *MPZ*, the corresponding nucleotide was replaced using the Vector NTI software (Invitrogen), and the designed vectors were synthesized by Gen Ray company. The pCDNA3.1/Native.MPZ and pCDNA3.1/Mutant.MPZ vectors were transformed into competent *Escherichia coli* Top 10 bacterial cells for amplification. Double digestion and q-PCR were assessed to confirm the presence of native and mutant *MPZ* gene in the designed location. Each construct was transiently and separately transfected to the CHO-K1 cells by exposing the cells to a 4:3 ratio of Lipofectamine 2000 (Invitrogen, USA)/vector combination for 6 h according to the manufacturer's instructions.

Quantitative estimation of native/mutant *MPZ* expression in CHO-K1 cells

CHO-k1 cells were seeded in a six-well plate and transfected the day after, and RNA extraction was performed with an RNA extraction kit (YTA, Iran) 24 h post-transfection. A total amount of 500 ng of the mRNA mixture was subjected to cDNA synthesis using the cDNA synthesis kit (YTA). The qPCR assay was conducted using primers corresponding to the second exon (Forward: 5′-ATG GCT CCT GGG GCT CCC TC-3′, Reverse: 5′-GAG ACC CAC TCA CTG GAC CAG AAG G-3′) and SYBR green Supermix (YTA) on a Corbett rotor gene 3000 real-

time system. A list of primers used in this work is presented in Table 1. The results were analyzed with Corbett Rotor-Gene 6000 software (version 1.7).

Immunofluorescence analyses

Cells were seeded in a chamber slide and transiently transfected with pCDNA/Native.MPZ and pCDNA/Mutant.MPZ. Cells were fixed with 4% paraformaldehyde (Merck, Germany) and exposed to 0.1% Triton X-100 (Sigma, USA) to permeabilize the cell membrane. After two washes with phosphate-buffered saline (PBS), the cells were incubated in a blocking solution containing 1% bovine serum albumin (BSA; Santa Cruz, USA) in PBS. Anti Myelin Protein Zero antibody (Abcam, ab31851) was then added at a ratio of 1:100 and incubated overnight at 4°C. After washing with PBS, the cells were incubated with the secondary Cy3 conjugated goat anti-rabbit antibody (Abcam, ab6939) in 1/2,000 dilution for 45 min. The nuclei were counterstained using 4′,6-diamidino-2-phenylindole (DAPI). Then the cells were covered with PBS and observed on a Nikon AZ100M epifluorescence microscope using AZ-Plan Flour 2x objective lenses (NA:0.2/WD:45 mm) with a DS-Fi1c digital camera at room temperature (20°C).

Statistical analysis

Data were analyzed using GraphPad Prism 6.0 software. To compare gene expression levels and the significance level between the two groups, a paired *T* test was used. $P < 0.05$ were also considered significant.

Results

Evaluation of patients with CMT1B

Genomic sample DNA was isolated from a total of 28 individuals out of 53 families who were considered as CMT1 according to the NVC results (5–30 m/s) and analyzed for *MPZ* mutations. The familial pedigree with an autosomal dominant pattern of inheritance is illustrated in Figure 2. For the two remaining families, the sequence analysis of the *MPZ* gene resulted in the detection of 89 T>C in the exon 2 (I30T) point mutation in one family (Figure 2) while the other family remained undiagnosed.

Molecular modeling

DOPE energies of all models were estimated by modeler 9 software. This energy is a statistical potential and an energy function obtained from the analysis of structures in PDB where the lower the DOPE energy of a model, the better structure it has. The least DOPE energy was related to model 2159. A Ramachandran plot of this model revealed that 94.5% of residues are energetically in the completely allowable region for backbone dihedral angles ψ and ϕ, and only 2.3% residues were in the almost allowed regions, and 3.2 were in the outlier region (picture not shown for brevity).

Molecular dynamic simulation

The averages of potential and temperature and backbone root-mean-square deviation (RMSD) of the native and mutant MPZ in the last 50 ns of the simulation are listed in Table 2. Figure 3 displays backbone RMSD plots of native and mutant MPZ during 100 ns MD simulation. The backbone RMSDs of both native and mutant MPZ proteins in simulation reach a plateau after 50 ns with a standard deviation of 4 and 1 Å respectively, therefore all analysis was accompanied in the last 50 ns of MD simulation. As shown in Table 2 and Figure 3, the results reveal that the simulations were converged, and the simulation times were enough, and both proteins formed a stable structure and reached equilibrium temperature and structure during the last 50 ns of MD simulation. The average RMSD of mutant MPZ is less than the native, and the high probability distribution function (PDF) occurs at a smaller value of RMSD for the mutant compared with native (Figure 3). Also, the potential energy of the mutant is more than the native, which indicates a higher instability after mutation in the MPZ protein (Table 2).

Table 2 shows the averages for the radius of gyration (Rg) for the native and mutant MPZ during the last 50 ns

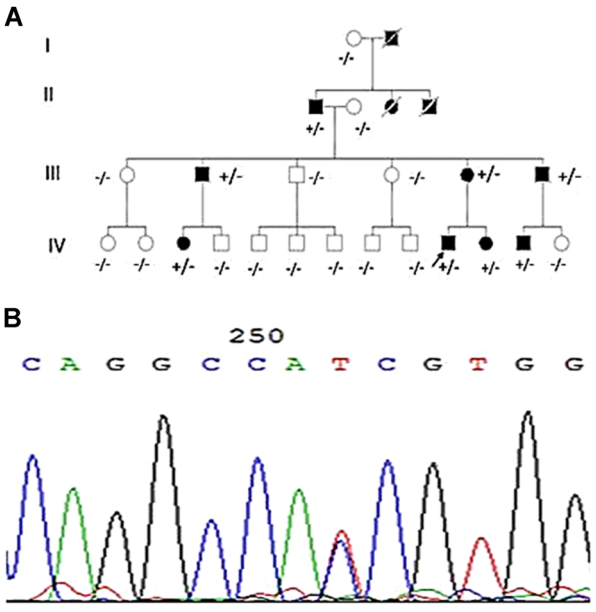

Figure 2 The I30T mutation. (A) The familial pedigree displays the autosomal dominance of the disease inheritance in four generations. (B) ABI sequencing results show 89 T>C mutation in the *MPZ* gene.

Table 2 Results of MD simulation of the native and mutated MPZ during the last 50 ns of 100 ns MD simulation.

MPZ protein	Potential energy (kJ/mol)	Temperature (K)	Backbone RMSD (nm)	Rg of protein (nm)	ASA (nm^2)
Native	−865,198 ± 1,030	299.98 ± 1.38	1.05 ± 0.04	1.78 ± 0.01	115.63 ± 3.47
Mutant	−865,170 ± 1,043	300 ± 1.4	0.94 ± 0.01	1.7 ± 0.008	113.17 ± 2.3

MD, molecular dynamics; MPZ, myelin protein zero; Rg, radius of gyration; RMSD, root mean square deviation.

of MD simulation. The Rg parameter explains the compactness of a specific protein or overall spread of the molecule in space. The Rg of the mutant protein is a little less than native protein, which means that the mutation leads to partial compaction in the extracellular part of MPZ. Furthermore, the mutation leads to the partial reduction of accessible surface area (ASA) of MPZ (Table 2) that is compatible with radius reduction (Figure 4).

Hydrogen bond (HB) analysis in the native and mutant is vital to recognize the stability and flexibility of the proteins. The average number of HBs between the extracellular part of MPZ and water during the last 50 ns of simulation decrease in the mutant MPZ (408) compared with the native protein (411) (Table 3). A decrease in the number of HBs between water and protein can lead to a decrease in the solubility of the mutant. In addition, the average of the number of intramolecular HB number (protein–protein) in MPZ in the native protein was about 133, while it was 129 in the mutant protein (Table 3). The lower number of HBs in the mutant results in the destabilization of mutant MPZ protein as compared to the native protein. This may also lead to abnormal folding of MPZ protein. The mutation also results in decreased HB formation in MPZ protein and between MPZ protein and water.

The tendency of secondary structural content is a vital component to study the structural behavior of a protein. The changes in secondary structure content in the native and mutant proteins are mentioned in Table 3. The mutation seems to lead to a reduction of the percentage of solid secondary structure (including α-helixes, β-sheaths, and turns) and partial increase of coil structure resulting in a partial reduction of secondary structure in the extracellular domain of MPZ protein. Indeed, the reduction of secondary structure content in the mutant is consistent with the reduction of the intramolecular HB in it.

Also, the average RMSF of residues of the mutant protein is less than the native protein suggesting a decrease of the flexibility of the mutant MPZ protein (Table 3). Figure 5 shows the backbone RMSF of native and mutant MPZ protein during the last 50 ns of MD simulation. This figure clearly illustrates a significant change in flexibility upon I30T mutation in the MPZ structure.

Additionally, a PCA was performed to investigate the collective motions of the native and mutant forms. PCA is one of the most extensively used tools to explore protein oscillations. The collective atomic motion of a protein is used as a parameter to understand the stability of the protein. This method engages diagonalization of the covariance matrix and provides the essential motion of the protein in phase space. This technique seeks to describe protein motions using a new basis set that directly redirects the combined motions undertaken by the system and also to separate large-scale cooperative motions. It has been

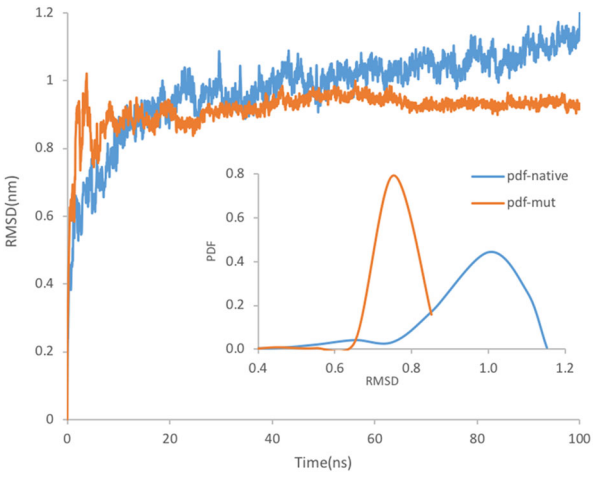

Figure 3 Backbone root-mean-square deviation (RMSD) of native and mutated myelin protein zero (MPZ) protein during 100 ns molecular dynamics (MD) simulation. The inset plot is the probability distribution function (PDF) of native and mutant structures.

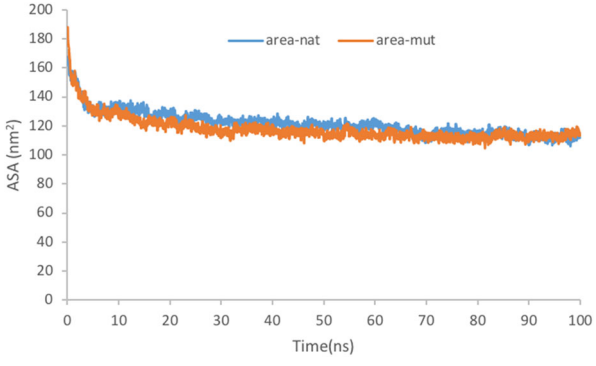

Figure 4 Accessible surface area (ASA) of the native and mutant myelin protein zero (MPZ) protein during 100 ns molecular dynamics (MD) simulation.

Table 3 Modification of the secondary structure content due to the mutation.

MPZ protein	Hbond-pro-pro	Hbond-pro-sol	Structure (%)	Coil (%)	Average of RMSF (nm)
Native	133.34 ± 6.47	411.8 ± 13.4	0.41	0.37	0.149
Mutant	129.81 ± 6.56	408.9 ± 13.6	0.39	0.38	0.095

MPZ, myelin protein zero; RMSD, root mean square deviation.

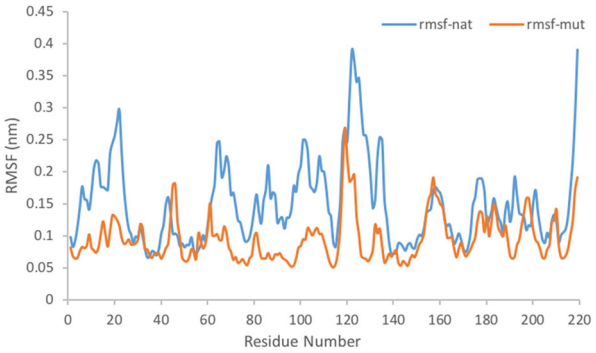

Figure 5 Backbone root-mean-square deviation (RMSF) of the native and mutated myelin protein zero (MPZ) during the last 50 ns of 100 ns molecular dynamics (MD) simulation.

suggested that the majority of the motions for proteins can be accounted for in the first few principal components (PCs). PCA is used to examine the global motions of protein into a few principal motions, characterized by eigenvectors. Therefore, the dynamics of a protein can be examined by projecting its atomic motion during an MD simulation onto its first few principal components. In this work, the principal components of protein motion were calculated as the eigenvectors of the Cα fluctuation covariance matrix. The basic Cα analysis gives a good image of the great concerted motions in the backbone. The first vector is the direction in which the group of atoms has the largest global mean square positional oscillation. The eigenvalue related to each vector signifies the change of the molecule along that vector (Grossfield et al., 2007). The first two eigenvalues (PC1 and PC2) were 2.12 and 0.56 respectively for the native protein and 0.626 and 0.202 for the mutant protein during the last 50 ns of MD simulation. Figure 6 shows projecting the Cα atom along PC1 versus projecting the Cα atom along PC2 for native and mutated MPZ structures during the last 50 ns of MD simulation. From the projection of PC1 and PC2 of the native and mutant, we could predict a cluster of stable states in the native and mutants. The results clearly show that the mutant protein shields an extensive range of phase spaces as compared to the native. The large increase in overall motion in the mutant reflects the prime cause of the deficiency of protein function. It seems that two states and a transition state (TS) through the folding of MPZ can be detected in this protein. It is obvious that mutation leads to a significant change in the folding of the MPZ protein.

To distinguish the conformational states and stability and folding of native and mutant, the Gibbs free energy landscape (FEL) was calculated via the first two principal components (PC1 and PC2) as reaction coordinates (Figure 7). The FEL can offer outstanding information about the different conformational states available to the protein in the

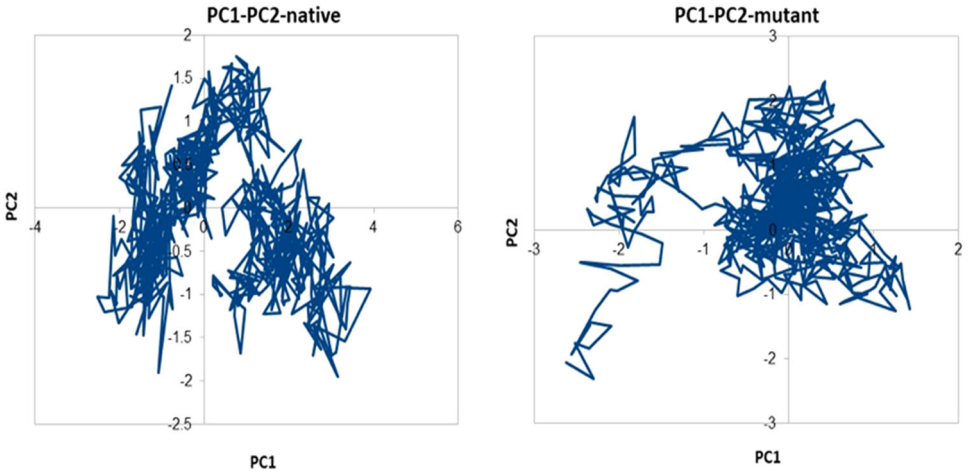

Figure 6 Projecting the Cα atom along PC1 versus projecting the Cα atom along PC2 for the native and mutated myelin protein zero (MPZ) structures during the last 50 ns of molecular dynamics (MD) simulation.

simulation. As can be seen in the figure, the native protein displayed a well-defined single global energy minima basin related to its conformational state, but the mutant explores broader global energy minima through a transition state. In the mutant, the native basin separates into two relative energy minima, offering the disruption of the native state. In other words, the existence of two energy minima in the conformational space realized in the mutant shows the partial destabilization of the protein.

Docking study

The MPZ ground state is achieved through the dimer or tetramer assembly of protein in the myelin sheath. Docking results of the native or mutant protein by the Haddock server have been summarized in Table 4. As expected, the mutation led to the diminution of the bonding power of mutant monomers and increased Haddock score. As shown in the table, Van der Waals's interactions become weaker and electrostatic interactions become more powerful. These results are logistic because of less Thr residue polarity comparing to that of Ile. The buried surface area is also decreased in the docking of mutant monomers to each other, which means weaker interaction of mutant monomers. As the CMT-1B is a heterozygous autosomal disease, the Schwann cells express both forms of the protein. Therefore, we performed a docking study between the native and mutant monomers, which suggested that the interactions between mutant and native monomers are weaker compared to the native monomers (or even mutant monomers to each other) (Table 4). These results are reasonable because the residue Isoleucine 1 (after signal peptide removal) is located at the surface of the extracellular domain and is necessary for monomer binding. Taken together, these data strongly indicate a possible malfunction in the heterologous dimerization of MPZ proteins.

In vitro expression of *MPZ*

CHO-K1 cells expressed the *MPZ* gene considerably with a $P = 0.0010$ and 0.0054 for pCDNA/Native.MPZ and pCDNA/Mutant.MPZ, respectively (Figure 8).

The I30T mutation affects the MPZ stability in the plasma membrane

To follow native and mutant MPZ intracellular trafficking, an immunofluorescence assay was conducted on transfected cells, and protein trafficking was tracked in a time-course approach. The diverse behavior of the native and mutant protein is displayed in Figure 9. Both proteins reached the plasma membrane with a slight conflict. Although the native MPZ reached the plasma membrane as soon as 8 h post-transfection, the mutant form exhibited a clear delay of up to 16 h. On the contrary, the native MPZ remained in the plasma membrane at least 40 h post-transfection, but the mutant protein disappeared from the plasma membrane before 32 h. These findings are the result of the whole transfected cells, which account for 5% of the population.

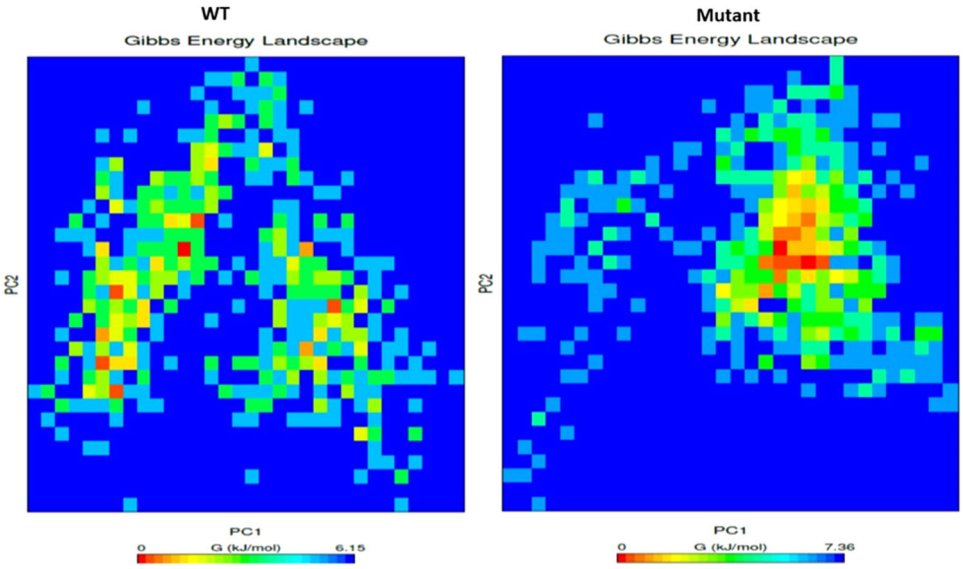

Figure 7 Free energy landscape of the native and mutated myelin protein zero (MPZ) protein during the last 50 ns of molecular dynamics (MD) simulation.

Table 4 Results of the docking study of the native and mutant MPZ monomers.

Docking parameter	Native-native	mutant-mutant	Native-mutant
HADDOCK score	−119.9 ± 6.2	−88.0 ± 7.9	−64.0 ± 5.2
Van der Waals energy	−64.9 ± 8.5	−39.5 ± 2.3	−45.6 ± 2.4
Electrostatic energy	−242.3 ± 28.3	−284.4 ± 31.3	−129.6 ± 35.5
Desolvation energy	−8.5 ± 3.5	8.4 ± 7.3	6.1 ± 4.1
Buried surface area	2338.1 ± 72.7	1131.3 ± 33.2	1520.5 ± 146.8
Z-score	−2.8	−1.8	−1.9
Cluster size	51	17	11

Discussion

Slight malfunctions in a nerve bundle that carry the signal to/from PNS brings about an insurmountable PNS system breakdown that affects multiple organs within a wide range (Bear, Connors, and Paradiso, 2009). CMT is a common neurological disorder that occurs due to mutations in several genes. Like all neuropathies, various environmental and intrinsic factors including oxidative stress, chemicals, drugs, transcription factors, aging, etc. can affect the prognosis of this disease (Braathen, 2012; Jami et al., 2015; Ahmadinejad et al., 2017; Reza and Ghahfarrokhi, 2017). The myelin sheath structured by these cells promotes signal transduction by reinforcing action potentials and probably other signaling factors that regulate the distribution of ion channels and other involved proteins (6, 9). Loss of integrity in the myelin sheath entails disruption of Schwann cell-axon communication and, ultimately, a failure in the function of several organs like muscles, skin, etc. (Rossor et al., 2013). The single transmembrane protein MPZ is responsible for motor and sensory malfunctions

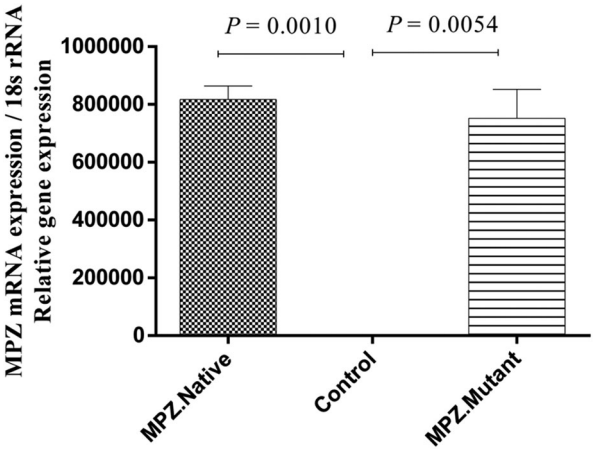

Figure 8 The native and mutant *MPZ* messenger RNA (mRNA) expression was evaluated 24 h post-transfection in CHO-K1 cells.

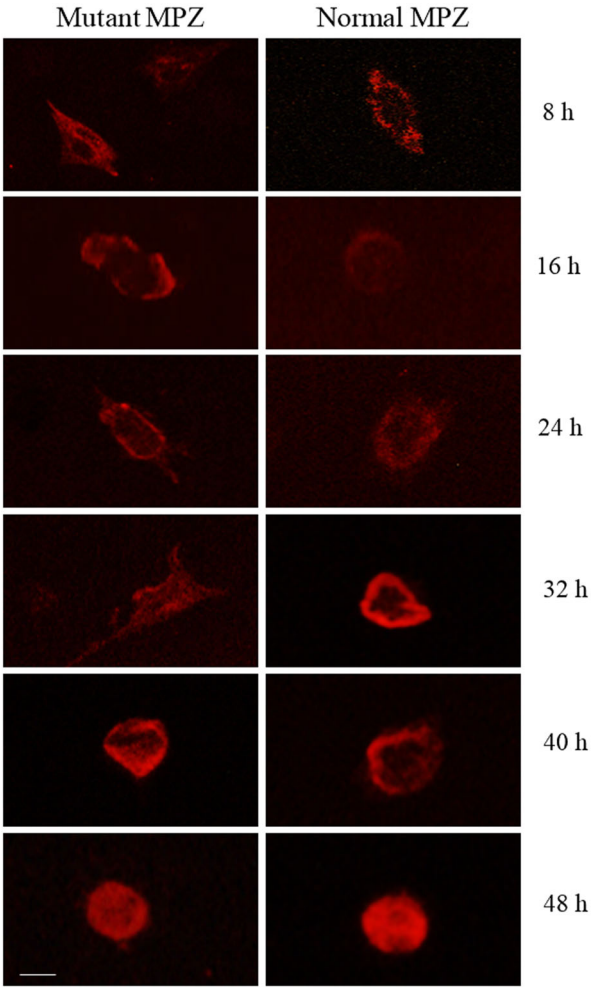

Figure 9 Following the native and mutant myelin protein zero (MPZ) protein trafficking in CHO-K1 cells. The native MPZ reached the plasma membrane by 8 h PT (post-transfection) and returned back to the cytosol after 48 h PT. The mutant MPZ has gained membrane residence by 16 h PT and returned back to the cytosol before 40 h PT. Each cell that is shown in each picture is the representative of the cellular population in the corresponding time frame (Bar 40 µm).

(Braathen et al., 2011). In this work, we studied the involvement of the *MPZ* gene in Iranian CMT patients via PCR amplification and sequencing of all of the *MPZ* exons, which resulted in the detection of several mutations, including substitution at the 30th residue of the MPZ protein (I30T). To better understand the molecular pathology and physicochemical properties of this mutation, we exerted a number of theoretical methods such as molecular dynamics simulation and docking simulation followed by in vitro validation.

Membrane proteins have been demonstrated to be challenging to study owing to their hydrophobic surfaces and elasticity. Therefore, very few membrane protein structures have been so far determined (Carpenter et al., 2008). The simulation methods are usually used to predict possible modifications in protein structure. Mandich et al. (2009) studied the effects of three mutations Tyr145fs (frameshift), Thr124Ala, Ser111Cys on the structure of the MPZ protein, and showed that these mutations have different effects (Mandich et al., 2009). Moreover, Shy et al. (2004) indicated that mutations in MPZ Ile30 lead to disruption of the tertiary structures and impaired self-adhesion of this protein, which further affects the myelin compaction capacity (Shy et al., 2004). Similarly, Liu et al. (2012) prepared the extracellular structure of the MPZ protein (Liu et al., 2012) by crystallography (PDB code: 3OAI), whose results were used in our study.

The in silico studies suggested that the mutation eventuates to the partial unfolding of the MPZ extracellular domain. In addition, the ConSurf server (http://consurf.tau.ac.il/2016/index_proteins.php) (Ashkenazy et al., 2010) shows that the isoleucine residue at the 30th position is highly conserved and therefore mutations in this site can be very vital. A 100 ns MD simulation was employed to examine the disruptive effects of I30T mutations on the conformational stability of MPZ protein.

In the present study, the extracellular part of MPZ protein was simulated in terms of the existence of water molecules and ions. The comparison of the extracellular domain of the mutant MPZ with the native revealed that the I30T mutation in MPZ protein leads to a decline of flexibility, radius of gyration, accessible surface area of the extracellular part, and partial denaturation. The I30T mutation also results in increased polarity (reduction of hydrophobicity) and the reduction of the accessible surface area. This finding is supported by the reduction of the number of intramolecular and intermolecular HBs in mutant MPZ and the reduction of solid secondary structures. Furthermore, PCA results showed that the folding and the first two principal components and free energy landscapes of mutant MPZ were different from the native MPZ protein. In addition, docking of native or mutant monomers to each other indicates that the mutation can lead to the destruction of the dimerization of MPZ protein. Our docking analyses revealed a very likely weakness in Van der Waals interactions, which is not surprising as the threonine residue is less hydrophobic than isoleucine. On the contrary, electrostatic interaction becomes stronger because threonine is more polar than isoleucine. Docking results indicated a lower capacity of hydrophobic interaction and decreased the potential of dimerization for the mutant protein compared to the normal one. This results in a critical defect in the integrity of the myelin and inefficiency of myelin structures to conduct the neural signals, and therefore, a sharp decrease in the nerve conductivity velocity.

These results are not similar to the results of Agrahari and George Priya Doss (2015), who previously suggested that I30T mutation can lead to the increment of RMSD and RMSF and radius of gyration and accessible surface area. This difference is probably because of our much longer simulations (100 ns) (thus more accurate) than their work (15 ns), although there are decreased numbers of HBs in both studies. In addition, they did not dock the native or mutant MPZ monomers to each other, while we showed that the Isoleucine substitution by threonine could lead to devastating the interacting properties of this immunoglobulin-like domain.

Taken together, our findings would help future research aiming to design next-generation drugs to amend the integration of mutant monomers in the membrane resulting in the treatment of CMT disease. Among the known mechanisms for the disease's molecular pathology, abnormal protein trafficking has gained attention for research in the field. Although there are no clear and strong correlations between protein trafficking and the disease's clinical phenotypes (Volpi et al., 2017), MPZ trafficking would seem to be a very important aspect of mechanistic studies. Misfolded transmembrane protein accumulation in the plasma membrane could cause loss of cell hemostasis and cell death. Accordingly, membrane proteins' folding is accurately monitored by membrane quality control systems (Babst, 2014). Cytoplasmic domain misfolding or an intrinsic untidiness of membrane proteins initiates the ubiquitination process and thus rapid clearance of the protein from the plasma membrane by the multivesicular body pathway (Babst, 2014). In our in vitro experiments, the I30T mutation in the MPZ protein seemed not to vigorously interfere with the intracellular trafficking but highly affected the protein stability in the plasma membrane. Rapid clearance of the mutant protein from the plasma membrane intercepts with the auto-immune response against Schwann cells and further inflammatory responses.

Slight disarrangement of myelin components could develop recurring disordered packing of two opposing membranes in the intermodal region with a frequent

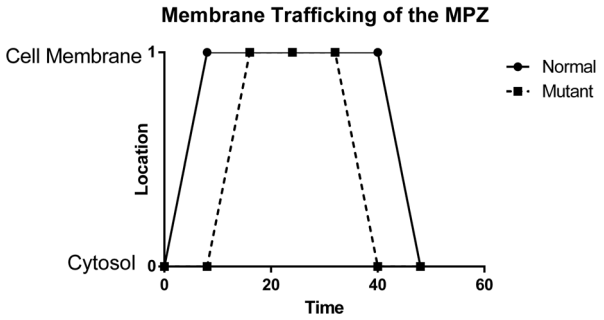

Figure 10 Schematic illustration of differences between native and mutant protein-membrane localization timeline. The instability of the mutant protein in the plasma membrane represents an altered tertiary structure of mutant myelin protein zero (MPZ) and its derivation from the native state.

detachment of membrane pairs (Kirschner et al., 1996). On the basis of the severity of the myelin disarrangement, hypomyelination, dysmyelination, or even axonal loss is an inevitable outcome. Incorporation of mutant MPZ in the myelin sheath could exert a dominant-negative effect on native MPZ proteins and consequently generates unpacked myelin wraps around the axons, which can be consistent with hypomyelination or dysmyelination of peripheral axons (Berger et al., 2007).

In our experimental studies, the mutant MPZ protein was transported to the cell membrane with a delay and returned back to the cytosol sooner than the native MPZ. The instability of the mutant MPZ in the membrane provides more evidence for the results of our simulation study suggesting the higher solubility and lower stability of mutant MPZ (Figure 10). The combination of these findings supports the conceptual premise that MPZ mutations disrupt the natural process and speed of protein trafficking.

As outlined above, the MPZ protein establishes hemophilic interactions in cis (with an MPZ protein in the same membrane) and trans (with an MPZ protein in the opposing membrane) patterns. It also interacts with other membrane proteins such as PMP22, GJB1 according to the STRING database (https://string-db.org). Therefore, the incorporation of these proteins in the Schwann cell membrane provides heterophilic interactions that facilitate the presence of MPZ protein in the myelin sheath. Presumably, lack of interacting proteins in CHO-K1 cells derived even the native MPZ protein back from the membrane after 48-hour post-transfection.

The validity of our data is based on one cellular model (CHO-K1), which might bring about complications in future studies on Schwann cell lines. Also, several questions remained unanswered at present. Future studies on the current topic with an emphasis on co-transfecting native-mutant MPZ protein should be undertaken to precisely manifest the difference between the trafficking of native and mutant MPZ protein. Future in vitro experiments on MPZ–MPZ interactions (adhesion tests) and MPZ–PMP22 interaction might clarify insecure localization of Mutant MPZ on the plasma membrane. Moreover, the analysis of intracellular responses to aggregated proteins like autophagy pathways and endoplasmic reticulum stress symptoms could provide a profound comprehension of disease mechanism and possible pathways and proteins to be targeted for future cell therapy treatments.

Conclusion

This study emphasizes the instability of the mutant MPZ in the plasma membrane and how this instability might affect the sophistication of the myelin sheath in peripheral nerves. Based on our in vitro and in silico analysis, the I30T mutation affects the stable localization of the MPZ protein in the plasma membrane. This knowledge may be of great benefit for future studies aiming to design molecular approaches for personalized cellular therapy.

Acknowledgment and funding

We thank all the staff and faculty members who helped us at SKUMS. This study was financially supported by the Shahrekord University of Medical Sciences, Iran (Grant Number 803).

Conflict of interest

The authors declare that there are no conflict of interests.

Availability of data and material

Further information and details on the data and materials will be made available on demand.

References

Agrahari A, George Priya Doss C (2015) Impact of I30T and I30M substitution in MPZ gene associated with Dejerine-Sottas syndrome type B (DSSB): a molecular modeling and dynamics. J Theor Biol 382: 23–33. https://doi.org/10.1016/j.jtbi.2015.06.019

Ahmadinejad F, Geir Møller S, Hashemzadeh-Chaleshtori M, Bidkhori G, Jami MS (2017) Molecular mechanisms behind free radical scavengers function against oxidative stress. Antioxidants (Basel, Switzerland) 6(3): 51. https://doi.org/10.3390/antiox6030051. Switzerland.

Ashkenazy H, Erez E, Martz E, Pupko T, Ben-Tal N (2010) ConSurf 2010: calculating evolutionary conservation in sequence and structure of proteins and nucleic acids.

Nucleic Acids Res 38(Suppl. 2): W529–33. https://doi.org/10.1093/nar/gkq399

Babst M (2014) Quality control at the plasma membrane: one mechanism does not fit all. J Cell Biol 205(1): 11–20, https://doi.org/10.1083/jcb.201310113

Bai Y, Wu X, Brennan KM, Wang DS, D'Antonio M, Moran J, Svaren J, Shy ME (2018) Myelin protein zero mutations and the unfolded protein response in Charcot Marie Tooth disease type 1B. Ann Clin Transl Neurol 5(4): 445–55, https://doi.org/10.1002/acn3.543

Bear FM, Connors WB, Paradiso MA (2009) Neuroscience exploring the brain. (3rd ed. Windsor Locks, CT: Lippincott Williams Wilkins.

Berendsen HJC, van der Spoel D, van Drunen R (1995) GROMACS: a message-passing parallel molecular dynamics implementation. Comput Phys Commun 91(1–3): 43–56, https://doi.org/10.1016/0010-4655(95)00042-E

Berger P, Niemann A, Suter U (2006) Schwann cells and the pathogenesis of inherited motor and sensory neuropathies (Charcot-Marie-Tooth disease). GLIA 54: 243–57, https://doi.org/10.1002/glia.20386

Berger P, Niemann A, Suter U (2007) Schwann cells and the pathogenesis of inherited motor and sensory neuropathies (Charcot-Marie-Tooth Disease). Glia 55(14): 1416–25, https://doi.org/10.1002/glia

Braathen GJ (2012) Genetic epidemiology of Charcot-Marie-Tooth disease. Acta Neurol Scand Suppl 126(193): iv-22, https://doi.org/10.1111/ane.12013

Braathen GJ, Sand JC, Lobato A, Høyer H, Russell MB (2011) Genetic epidemiology of Charcot-Marie-Tooth in the general population. Eur J Neurol 18(1): 39–48, https://doi.org/10.1111/j.1468-1331.2010.03037.x

Burns TM, Mauermann ML (2011) The evaluation of polyneuropathies. Neurology 76(7 Suppl 2): S6-13.

Carpenter EP, Beis K, Cameron AD, Iwata S (2008) Overcoming the challenges of membrane protein crystallography. Curr Opin Struct Biol 18: 581–6, https://doi.org/10.1016/j.sbi.2008.07.001

DiVincenzo C, Elzinga CD, Medeiros AC, Karbassi I, Jones JR, Evans MC, Braastad CD, Bishop CM, Jaremko M, Wang Z, Liaquat K, Hoffman CA, York MD, Batish SD, Lupski JR, Higgins JJ (2014) The allelic spectrum of Charcot-Marie-Tooth disease in over 17,000 individuals with neuropathy. Mol Genet Genomic Med 2(6): 522–9, https://doi.org/10.1002/mgg3.106

Gelpi J, Hospital A, Goñi R, Orozco M (2015) Molecular dynamics simulations: advances and applications. Adv Appl Bioinform Chem 8: 37–47, https://doi.org/10.2147/AABC.S70333

Ghanavatinejad F, Fard Tabrizi ZP, Omidghaemi S, Sharifi E, Møller SG, Jami MS (2019) Protein biomarkers of neural system. J Otol 14(3): 77–88, https://doi.org/10.1016/j.joto.2019.03.001

Ghasemi-Dehkordi P, Allahbakhshian-Farsani M, Abdian N, Mirzaeian A, Saffari-Chaleshtori J, Heybati F, Mardani G, Karimi-Taghanaki A, Doosti A, Jami MS, Abolhasani M, Hashemzadeh-Chaleshtori M (2015) Comparison between the cultures of human induced pluripotent stem cells (hiPSCs) on feeder-and serum-free system (Matrigel matrix), MEF and HDF feeder cell lines. J Cell Commun Signal 9(3): 233–46, https://doi.org/10.1007/s12079-015-0289-3

Grossfield A, Feller SE, Pitman MC (2007) Convergence of molecular dynamics simulations of membrane proteins. Proteins 67(1): 31–40, https://doi.org/10.1002/prot.21308

Hess B, Bekker H, Berendsen HJC, Fraaije JGEM (1997) LINCS: a linear constraint solver for molecular simulations. J Comput Chem 18(12): 1463–72, https://doi.org/10.1002/(SICI)1096-987X(199709)18:12<1463::AID-JCC4>3.0.CO;2-H

Hess B, Kutzner C, van der Spoel D, Lindahl E (2008) GRGMACS 4: algorithms for highly efficient, load-balanced, and scalable molecular simulation. J Chem Theory Comput 4(3): 435–47, https://doi.org/10.1021/ct700301q

Jami M-S, Salehi-Najafabadi Z, Ahmadinejad F, Hoedt E, Chaleshtori MH, Ghatrehsamani M, Neubert TA, Larsen JP, Møller SG (2015) Edaravone leads to proteome changes indicative of neuronal cell protection in response to oxidative stress. Neurochem Int 90: 134–41, https://doi.org/10.1016/j.neuint.2015.07.024

Kirschner DA, Szumowski K, Hoogendijk JE (1996) Inherited demyelinating peripheral neuropathies: relating myelin packing abnormalities to P0 molecular defects. J Neurosci Res 46: 502–8.

Lindahl E, Hess B, van der Spoel D (2001) GROMACS 3.0: a package for molecular simulation and trajectory analysis. J Mol Model 7: 306–17, https://doi.org/10.1007/S008940100045

Liu Z, Wang Y, Yedidi RS, Brunzelle JS, Kovari IA, Sohi J, Kamholz J, Kovari LC (2012) Crystal structure of the extracellular domain of human myelin protein zero. Proteins 80: 307–13, https://doi.org/10.1002/prot.23164

Mahmoudian-Sani MR, Mehri-Ghahfarrokhi A, Hashemzadeh-Chaleshtori M, Saidijam M, Jami MS (2017) Comparison of three types of mesenchymal stem cells (bone marrow, adipose tissue, and umbilical cord-derived) as potential sources for inner ear regeneration. Int Tinnitus J 21(2): 112–21, https://doi.org/10.5935/0946-5448.20170022

Mandich P, Fossa P, Capponi S, Geroldi A, Acquaviva M, Gulli R, Ciotti P, Manganelli F, Grandis M, Bellone E (2009) Clinical features and molecular modelling of novel MPZ mutations in demyelinating and axonal neuropathies. Eur J Human Genet 17(9): 1129–34, https://doi.org/10.1038/ejhg.2009.37

Mansourian M, Madadkar-Sobhani A, Mahnam K, Fassihi A, Saghaie L (2012) Characterization of adenosine receptor in its native environment: insights from molecular dynamics simulations of palmitoylated/glycosylated, membrane-integrated human A2B adenosine receptor. J Mol Model 18(9): 4309–24, https://doi.org/10.1007/s00894-012-1427-y

Mehri-Ghahfarrokhi A, Pourteymourfard-Tabrizi Z, Farrokhi E, Chaleshtori MH, Jami MS (2019) Increased levels of miR-124 in human dental pulp stem cells alter the expression of neural markers. J Otol 14: 121–127, https://doi.org/10.1016/J.JOTO.2019.04.001

Mosaeilhy A, Mohamed MM, C GPD, El Abd HSA, Gamal R, Zaki OK, Zayed H (2017) Genotype-phenotype correlation in 18 Egyptian patients with glutaric acidemia type I. Metab Brain Dis 32(5): 1417–26, https://doi.org/10.1007/s11011-017-0006-4

Niemann A, Berger P, Suter U (2006) Pathomechanisms of mutant proteins in charcot-marie-tooth disease. NeuroMolecular Med 8: 217–41, https://doi.org/10.1385/NMM:8:1-2:217

Rafiee F, Pourteymourfard-Tabrizi Z, Mahmoudian-Sani MR, Mehri-Ghahfarrokhi A, Soltani A, Hashemzadeh-Chaleshtori M, Jami MS (2019) Differentiation of dental pulp stem cells into neuron-like cells. Int J Neurosci 1–10, https://doi.org/10.1080/00207454.2019.1664518

Reza M, Ghahfarrokhi AM (2017) MicroRNAs: effective elements in ear-related diseases and hearing loss. Eur Arch Otrhinolaryngol 6: 52, https://doi.org/10.1007/s00405-017-4470-6

Rossor AM, Polke JM, Houlden H, Reilly MM (2013) Clinical implications of genetic advances in charcot-marie-tooth disease. Nat Rev Neurol 9(10): 562–71, https://doi.org/10.1038/nrneurol.2013.179

Saffar B, Mehri Ghahfarrokhi A, Mahnam K, Mobini-Dehkordi M (2015) Improvement of Cd2+ uptake ability of SmtA protein by Lys/Cys mutation; experimental and theoretical studies. J Biomol Struct Dyn 33(11): 2347–59, https://doi.org/10.1080/07391102.2015.1054431

Šali A, Blundell TL (1993) Comparative protein modelling by satisfaction of spatial restraints. J Mol Biol 234(3): 779–815, https://doi.org/10.1006/jmbi.1993.1626

Shy ME (2004) Phenotypic clustering in MPZ mutations. Brain 127(2): 371–84, https://doi.org/10.1093/brain/awh048

Thirumal Kumar D, Eldous HG, Mahgoub ZA, George Priya Doss C, Zayed H (2018) Computational modelling approaches as a potential platform to understand the molecular genetics association between Parkinson's and Gaucher diseases. Metab Brain Dis 33(6): 1835–47, https://doi.org/10.1007/s11011-018-0286-3

Van Der Spoel D, Lindahl E, Hess B, Groenhof G, Mark AE, Berendsen HJC (2005) GROMACS: fast, flexible, and free. J Comput Chem 26: 1701–18, https://doi.org/10.1002/jcc.20291

van Oss CJ (2008) Chapter three the extended DLVO theory. Interface Sci Technol 31–48, https://doi.org/10.1016/S1573-4285(08)00203-2

Verhamme C (2010). Charcot-Marie-Tooth type 1A: natural course, pathophysiology and treatment. Chapeter 4-6, ISBN 9789081608114.

Volpi VG, Touvier T, D'Antonio M (2017) Endoplasmic reticulum protein quality control failure in myelin disorders. Front Mol Neurosci 9: 162, https://doi.org/10.3389/fnmol.2016.00162

Van Zundert GCP, Rodrigues JPGLM, Trellet M, Schmitz C, Kastritis PL, Karaca E, Melquiond ASJ, van Dijk M, de Vries SJ, Bonvin AMJJ (2016) The HADDOCK2.2 web server: user-friendly integrative modeling of biomolecular complexes. J Mol Biol 428(4): 720–5, https://doi.org/10.1016/j.jmb.2015.09.014

Received 22 May 2019; accepted 14 November 2019.
Final version published online 4 December 2019.